

A Soft-Rigid Hybrid Gripper With Lateral Compliance and Dexterous In-Hand Manipulation

Wenpei Zhu , Chenghua Lu, Qule Zheng, Zhonggui Fang , Haichuan Che, Kailuan Tang, Mingchao Zhu , Sicong Liu , and Zheng Wang , *Senior Member, IEEE*

Abstract—Soft grippers are receiving growing attention due to their compliance-based interactive safety and dexterity. Hybrid gripper with soft actuators enhanced by rigid constraints is receiving growing attention in soft gripper design. With rigid structural components actuated by soft actuators, they could achieve excellent grasping adaptability and payload while also being easy to model and control with conventional kinematics. However, existing works were mostly focused on achieving superior payload and perception with simple planar workspaces, resulting in far less dexterity compared with conventional grippers. In this work, we took inspiration from the human metacarpophalangeal (MCP) joint and proposed a new hybrid gripper design with eight independent muscles. It was shown that adding the MCP complexity was critical in enabling a range of novel features in the hybrid gripper, including in-hand manipulation, lateral passive compliance, as well as new control modes. A prototype gripper was fabricated and tested on our proprietary dual-arm robot platform with vision-guided grasping. With very lightweight pneumatic bellows soft actuators, the gripper could grasp objects

over 20 times its weight with lateral compliance. Using the dual-arm platform, highly anthropomorphic dexterous manipulations were demonstrated using two hybrid grippers, from tug of war on a rigid rod to passing a soft towel between two grippers using in-hand manipulation. Matching the novel features and performance specifications of the proposed hybrid gripper, the underlying modeling, actuation, control, and experimental validation details were also presented, offering a promising approach to achieving enhanced dexterity, strength, and compliance in robotic grippers.

Index Terms—Dual-arm manipulation, grasping dexterity, in-hand manipulation, modeling and control, soft grippers.

I. INTRODUCTION

GRIPPER is the key component for robots to interact with the environment [1]. Gripper design faces challenges when robots leave factories and perform activities of daily life (ADL) in domestic environments [2]. ADLs raise challenges [3] that call for inherent compliance and even in-hand manipulation of the robotic grippers, to handle delicate objects and adapt to unknown environments [4], [5].

Adding compliance to the kinematic chain has been extensively explored to provide compliance to rigid grippers [5]. Direct motor-driven grippers with compliance prefer to use a passive mechanism, such as a spring to enhance environmental adaptability [6], [7], with the compliance determined by the mechanical property of the mechanism, less likely to be modified or controlled once manufactured [see Fig. 1(a1)]. Tendon-driven grippers with compliance combine compliance and high-DOF finger joints using tendon actuation [see Fig. 1(a2)], but each additional DOF requires the addition of one or two motors, adding to the overall weight and volume of the system as the flexibility of the system increase [8]–[11].

Recent trends in developing soft grippers using various soft materials achieved inherent and unparalleled passive compliance [12]–[20], but also suffer from highly limited control bandwidth and grasping force, being challenging to model and control in real-time, mainly due to their soft material body without rigid kinematics. A recent trend of hybrid gripper designs using soft actuators augmented in rigid links [21]–[25] combines the advantages of soft gripper compliance and rigid kinematics [see Fig. 1(a3)]: the inherent softness of actuators enables the

Manuscript received 4 January 2022; revised 31 May 2022; accepted 16 July 2022. Recommended by Technical Editor A. Dani and Senior Editor G. Alici. This work was supported in part by the Science, Technology, and Innovation Commission of Shenzhen Municipality under Grant ZDSYS20200811143601004, in part by Guangdong Basic and Applied Basic Research Foundation under Grant 2021A1515110658, in part by NSFC under Grant 51975268, in part by the Guangdong Provincial Key Laboratory of Human-Augmentation and Rehabilitation Robotics in Universities, in part by Southern Marine Science and Engineering Guangdong Laboratory (Shenzhen), and in part by SUSTECH Education Endowment Fund. (Wenpei Zhu and Chenghua Lu are co-first authors.) (Corresponding author: Zheng Wang.)

Wenpei Zhu, Chenghua Lu, Qule Zheng, Zhonggui Fang, Haichuan Che, Kailuan Tang, Sicong Liu, and Zheng Wang are with the Shenzhen Key Laboratory of Biomimetic Robotics and Intelligent Systems, Department of Mechanical and Energy Engineering, the Guangdong Provincial Key Laboratory of Human Augmentation and Rehabilitation Robotics in Universities, and the Department of Mechanical and Energy Engineering, Southern University of Science and Technology, Shenzhen 518055, China (e-mail: 11930368@mail.sustech.edu.cn; luchenghua18@mails.ucas.ac.cn; 12049017@mail.sustech.edu.cn; 11930523@mail.sustech.edu.cn; 11810402@mail.sustech.edu.cn; tangkl@mail.sustech.edu.cn; liusc@sustech.edu.cn; wangz@sustech.edu.cn).

Mingchao Zhu is with the Changchun Institute of Optics, Fine Mechanics and Physics, University of Chinese Academy of Sciences, Beijing 100049, China (e-mail: mingchaozhu@gmail.com).

This article has supplementary material provided by the authors and color versions of one or more figures available at <https://doi.org/10.1109/TMECH.2022.3195985>.

Digital Object Identifier 10.1109/TMECH.2022.3195985

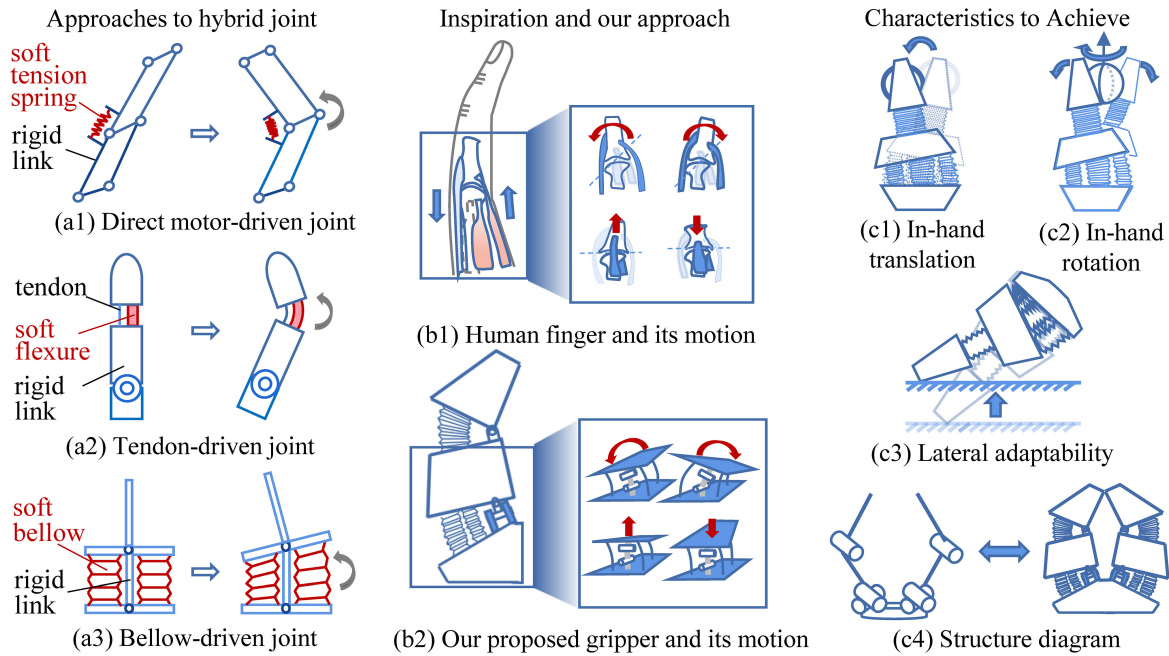


Fig. 1. Concept of the proposed gripper design. (a1) Direct motor-driver joint achieves compliance by using soft spring [6]. (a2) Tendon-driven joint achieves compliance by using soft flexure [10]. (a3) Bellow-driven soft joint achieves compliance by soft bellow actuators [21]. (b1) Human finger can achieve FEAA with MCP joint. (b2) Our proposed gripper can achieve similar motions to a human's finger in (b1) as the PSAJ can achieve FEAA. (c1) and (c2) Our proposed gripper has enhanced in-hand manipulability, which can achieve different directive motions of a ball in the gripper. (c3) When our proposed gripper touches the surface with the lateral side, the gripper can adapt to the surface without breaking the environment or itself. (c4) Our proposed gripper has a simple structure diagram, whose kinematics can be solved as a rigid robot.

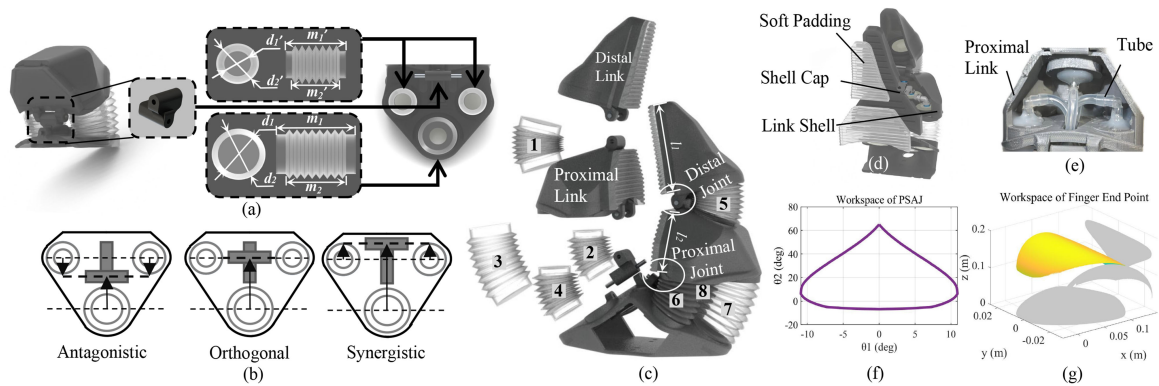


Fig. 2. Details of the PSAJ and BHG-6. (a) Composition of PSAJ. (b) Three available options for actuator distribution. (c) Name of links [11] and number of bellows. The black color refers to rigid links and the gray color refers to soft actuators. (d) Three layers of gripper. (e) Internal tube arrangement of proximal link. (f) Workspace of PSAJ. (g) Workspace of gripper's finger endpoint.

gripper's passive adaptability and compliance while the rigid structure enabling precise modeling and control [21], [23], [24]. However, existing hybrid grippers are mainly focused on high payload [21], [25] and perception [23], [25], with highly limited dexterity and lateral adaptability [21], [23]–[25].

In this work, we proposed a novel dexterous hybrid gripper design with lateral compliance and manipulation dexterity, not only to improve the bandwidth and payload limited for soft grippers but also to achieve real-time-capable modeling and control. The gripper is comprised of pneumatic-driven soft-robotic joints augmented into rigid structural constraints inspired by the human metacarpophalangeal (MCP) joint (2-DOF compliant motion) and the proximal interphalangeal (PIP) joint

(1-DOF compliant motion), with enhanced performances on lateral adaptability as well as in-hand manipulability. The main contributions of this article can be summarized as follows:

- 1) Proposed a novel pneumatic synergistic alignment joint (PSAJ) inspired by the human MCP joint, using three independently actuated, synergistically configured soft muscles to achieve 2-DOF rotation along with pitch and yaw axis, constrained by a rigid universal joint, with passive compliance in both bending directions.
- 2) Proposed a novel 6-DOF bio-inspired hybrid gripper (BHG-6) with PSAJ in each finger, achieving dexterous in-hand manipulation of objects, as well as improved payloads.

- 3) Exploiting the lateral compliance, the proposed gripper was demonstrated in a compliance-centric grasping approach of planar soft objects against flat rigid surfaces, where the BHG-6 gripper relied on its lateral compliance to pick up sheet-form objects, such as a towel.

The remainder of this article is organized as follows. Section II presents the concept and design of the PSAJ and the BHG-6 gripper, taking inspiration from the human MCP joint. Section III presents the modeling, control as well as high-level visual rendering and simulation, followed by the experimental validations and demonstration in Section IV. Finally, Section V concludes this article.

II. DESIGN OF THE BHG-6 GRIPPER

A. Inspiration and Design Concept

The human finger joint offers abundant inspiration for robot gripper design. The flexion/extension/abduction/adduction (FEAA) motions of the finger are largely enabled by the MCP joint, with the left-and-right swing of the forefinger realized by pulling the tendons at both ends; while the knuckles provide motion restrictions. In addition to performing flexion and extension, the dorsal interosseous muscle and palmar interosseous muscle also enable abduction and adduction [see Fig. 1(b1)]. Therefore, the joint achieves 2-DOF motion within a highly confined space with both axial and lateral compliance.

Inspired by the MCP joint, we proposed a PSAJ design of the soft robotic joint, a pneumatic soft-rigid hybrid joint that can realize bending and swinging motion [see Fig. 1(b2)], with all three soft actuator muscles placed synergistically on the outer side to the joint, achieving different control modes for various types of grasping operations. Based on the PSAJ, we proposed a 6-DOF symmetrical hybrid gripper BHG-6 with a hybrid structure (rigid kinematics and soft joints) achieving multidirectional compliance [see Fig. 1(c)]. In contrast to rigid grippers where each DOF usually requires a separate driving motor and, therefore, increases the system weight and complexity rather linearly, the proposed BHG-6 adopted a pneumatic actuation approach, where all soft muscles share the same pair of pumps (one compressor and one vacuum), and each additional DOF only requires two compact-sized valves. As a result, the 6-DOF design could be matched with a relatively compact pneumatic control system, and the rule of thumb is the more DOF required, the more advantageous this approach will be regarding the overall system weight and size. In addition, thanks to its hybrid structure, the BHG-6 has a rigid kinematic structure together with its soft muscle joints, allowing it to be modeled and visualized in a highly computationally efficient manner, ideal for real-time control with MCU platforms.

B. Design and Modeling of PSAJ

The proposed PSAJ joint consists of two rigid links. Abduction/adduction was enabled by a universal pin hinge while limiting lateral translations, to achieve precise motion, as shown in Fig. 2(a). For lightweight and performance coherence of the actuators, the blow-molded soft bellows introduced in our

TABLE I
GEOMETRY OF BELLOWS AND LINKS

	Overall dimension	175 mm × 160 mm × 80 mm
m_1	Length of large bellow's elbow-cover area	70 mm
m_2	Length of large bellow	44 mm
m_1'	Length of small bellow's elbow-cover area	50 mm
m_2'	Length of small bellow	39 mm
d_1	Diameter of big bellow	30.5 mm
d_2	Diameter of big bellow's elbow-cover area	23 mm
d_1'	Diameter of small bellow	37.56 mm
d_2'	Diameter of small bellow's elbow-cover area	32.37 mm
l_1	Length of distal link	51.12 mm
l_2	Length of proximal link	70.56 mm

previous work [20] were adopted as soft actuators to drive rigid links. The material of the actuator is ethylene-vinyl acetate copolymer. They could yield a high payload-to-weight ratio as well as an excellent expansion ratio of 2.5:1 [20].

The PSAJ design has two orthogonal DOFs, abduction/adduction and flexion/extension. Following the hybrid design approach with soft actuators augmented into rigid constraints, we use three soft bellows actuators, one large actuator for the main flexion DOF, and two symmetrical smaller actuators for actuation of abduction/adduction. They are all mounted on a common base with the universal joint, such that joint elongation is restricted by the universal joint, only allowing two-way bending. Here, a synergistic alignment was chosen over the antagonistic or orthogonal approaches [see Fig. 2(b)], to achieve abduction/adduction while enabling a “power mode” in the flexion direction, where all three muscles could be actuated simultaneously to get the maximum grasping force. This leads to a dedicated “power mode” in grasping control. Experimental results show that under synergistic alignment, the payload can be improved by about 20% by inflating all actuators compared to inflating only actuator 3. Details can be seen in the video.

To improve compactness, two smaller diameter lateral muscles were used instead of one large muscle with a similar overall cross-sectional area, to ensure sufficient flexion force in grasping, as shown in Fig. 2(a). Symmetrical small-sized actuators realize swing motion, the main large-sized actuator realizes opening-and-closing motion. The detailed size of the two kinds of actuators is shown in Table I. It is worth noting that the dimensions of the two types of bellows are not specifically unique, they will determine other performance indices, such as bending range, payload, etc., without losing generality. In this configuration, the workspace analysis of the PSAJ joint is shown in Fig. 2(f), with a maximum opening distance of 166 mm between the two finger tips.

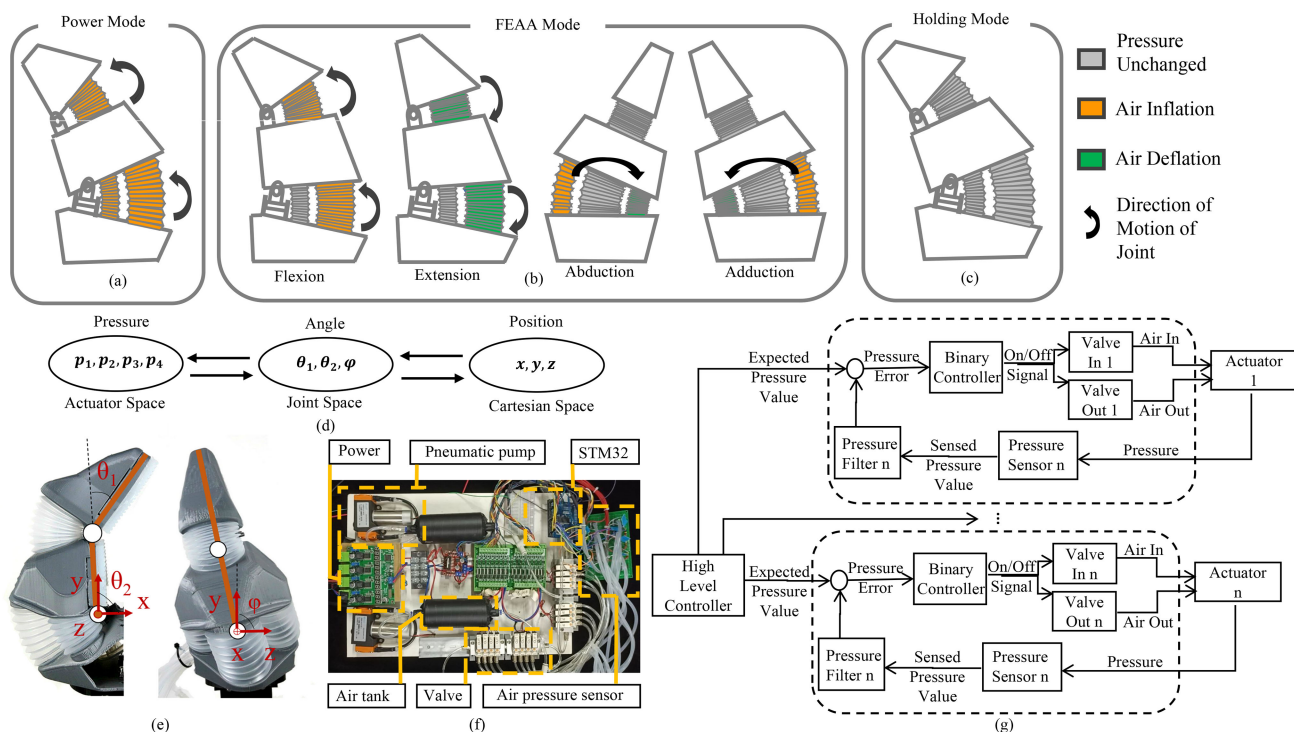


Fig. 3. Low-level control of gripper. (a)–(c) Control modes of the gripper and the mapping between bellow's motion with color. (d) Space transformation of pressure, angle, and position. (e) Kinematics schematic when gripper rotates in x - y plane and y - z plane. (f) Pneumatic control system, total weight 3.1 kg. (g) Control system diagram.

C. Design and Modeling of BHG-6

The proposed BHG-6 design adopts a hybrid symmetrical two-finger design [see Fig. 2(c)] consisting of following three layers.

- 1) *Layer 1-Rigid links and inner piping*: The 3D-printed rigid components consist of three different types: distal link, proximal link, and gripper base. The distal link and the proximal link are joined by a general pin hinge, and the proximal link and the gripper base are joined by a universal pin hinge, allowing both centric and lateral flexing [see Fig. 2(c)]. The finger links are designed to be hollow for weight reduction and passing pipes [see Fig. 2(e)].
- 2) *Layer 2-Soft actuators*: The gripper consists of four large-sized bellows and four small-sized bellows, achieving high-payload actuation while preserving passive compliance, as shown in Fig. 2(d). Bellow 1 and 5 drive the distal joint; bellow 2,3,4,6,7,8 drive the PSAJ [see Fig. 2(c)].
- 3) *Layer 3-Contact surface*: To improve contact friction, the contact surface of each finger is covered with soft padding molded from silicone rubber (Ecoflex-0030) with symmetric texture in both directions [see Fig. 2(d)]. When grasping, the flexible contact surface can increase the contact area and increase contact friction, so that improving grasping stability.

Finally, the workspace analyses of the PSAJ [see Fig. 2(f)] and the BHG-6 gripper [see Fig. 2(g)] are presented, with the tip

joint movement range of the fingertip measured by simulation, showing the large range of lateral motion available for dexterous grasping operations.

III. KINEMATICS AND CONTROL OF THE GRIPPER

A. Low-Level Control of the Gripper

1) *Control Modes*: The need for different gripper performances, such as grasping force or control simplicity, varies according to different tasks. Facing the various need, the synergistic aligned PSAJ provided us possibilities to deal with the need by only changing the actuation logic. Here, we introduce three working modes to deal with different grasping applications, which are as follows.

Mode 1 ("Power mode"): This mode is designed to provide a large grasping force in power grasping. With the synergistic alignment of actuators, by inflating all actuators simultaneously in closing the gripper, we could maximize the output grasping force for high payloads [see Fig. 3(a)]. No control distinction of muscles is available in this mode. Lateral motion is not actively enabled, although passively the gripper remains inherently compliant to bidirectional external disturbances.

Mode 2 ("FEAA mode"): The PSAJ could independently control the two DOFs to perform very dexterous motions combining flexion/extension and abduction/adduction, with the pressure of actuator 3 determining the open–close angle of the PSAJ; the pressure difference of actuators 2 and 4 results in lateral rotation [see Fig. 3(b)].

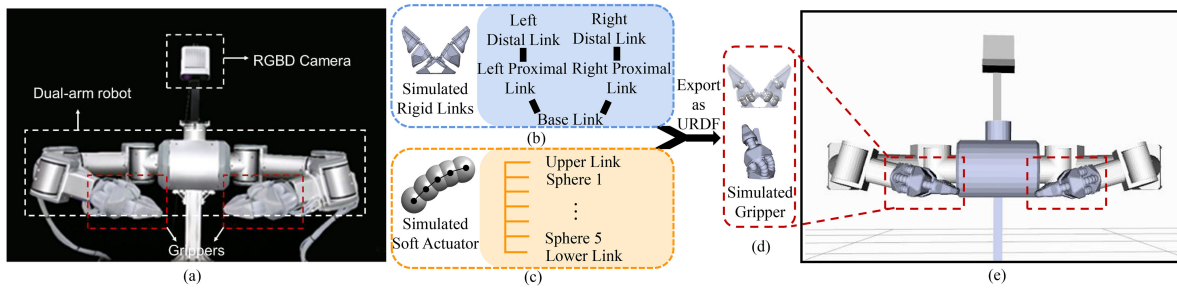


Fig. 4. Platform introduction for vision-based grasping towels. (a) Experimental platform in reality. The system includes a dual-arm robot, two grippers, and an RGB-D camera. (b)–(d) Gripper model for simulation and visualization. (b) Links, marked using blue color, can be modeled naturally for its rigid structure. (c) Soft actuator is separated into several parts. Each part is represented using a sphere (see text for detailed description). (d) Final performance of our simulation model shown in Rviz. (e) Experimental platform in Rviz.

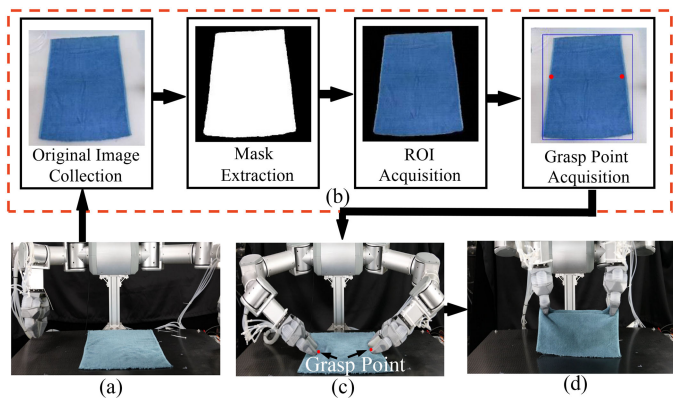


Fig. 5. Process of vision-based accurate grasping. (a) Camera is recognizing the grasping point. (b) Process of recognizing the midpoint of the edge of the towel. (c) Grippers perform the grasping action. (d) Grippers lift the towel.

Mode 3 (“Holding mode”): Besides the two modes above, we also proposed a mode to stabilize the finger’s position. In this mode, valves are shut to lock down the air in the actuators. When the external force is removed, the finger will recover to its original position before applying an external force, which will stabilize the grasping [see Fig. 3(c)].

2) Kinematics and Pressure Control Mapping: The control workflow of the finger mentioned in mode 2 is shown in Fig. 3(d), by first setting up the relationship between the endpoint of gripper $\{x, y, z\}$, (Cartesian space position of the fingertip), and joint angle $\{\theta_1, \theta_2, \phi\}$ (representing the rotation angle of the top joint in the x - y plane, root joint in the x - y plane, root joint in the y - z plane, respectively). Then, the relationship between joint angle and actuator pressure $\{p_1, p_2, p_3, p_4\}$ (pressure of four actuators, in order from top to root and from left to right.) is studied [see Fig. 3(d)].

Benefiting from the hybrid structure, compared to purely soft-bodied grippers usually requiring finite-element simulation/optimization for modeling and control, our gripper can be modeled analytically from its rigid kinematics.

From the x - y plane, as shown in Fig. 3(e), the position of the fingertip can be described as

$$\mathbf{P}_e = \begin{pmatrix} l_1 \cos(\theta_2 - \theta_1) + l_2 \cos \theta_2 \\ l_1 \sin(\theta_2 - \theta_1) + l_2 \sin \theta_2 \\ 0 \end{pmatrix}. \quad (1)$$

When P_e is rotated around the x -axis, the position becomes

$$\mathbf{P}'_e = \mathbf{R}_x \mathbf{P}_e = \begin{pmatrix} l_1 \cos(\theta_2 - \theta_1) + l_2 \cos \theta_2 \\ l_1 \sin(\theta_2 - \theta_1) \cos \phi + l_2 \sin \theta_2 \cos \phi \\ l_1 \sin(\theta_2 - \theta_1) \sin \phi + l_2 \sin \theta_2 \sin \phi \end{pmatrix} \quad (2)$$

where R_x represents the rotation matrix around the x -axis.

For joint angle control, we linearized the mapping between joint angle and pressure method to control the joint angle following a similar approach reported previously [23], [25] and the model proposed in previous work [26]. For Mode 2 (FEAA), the rotation angle of the tip joint θ_1 is regarded as a linear function of pressure at actuator 1, which can be presented as $\theta_1 = k_1 p_1 + b_1$. Similarly, the open-close angle $\theta_2 = k_2 p_3 + b_2$, lateral rotational angle $= k_3 \Delta p_{24} + b_3$, where Δp_{24} denotes the difference of pressure between actuators 2 and 4. Substituting the linear equations in (2), with k the slope in the linear relationship between pressure and joint angle, and b the corresponding intercept, (2) becomes

$$\mathbf{P}'_e = \begin{pmatrix} l_1 c(k_2 p_3 - k_1 p_1 + b_2 - b_1) + l_2 c(k_2 p_3 + b_2) \\ l_1 s(k_2 p_3 - k_1 p_1 + b_2 - b_1) c(k_3 \Delta p_{24} + b_3) \\ + l_2 s(k_2 p_3 + b_2) c(k_3 \Delta p_{24} + b_3) \\ l_1 s(k_2 p_3 - k_1 p_1 + b_2 - b_1) s(k_3 \Delta p_{24} + b_3) \\ + l_2 s(k_2 p_3 + b_2) s(k_3 \Delta p_{24} + b_3) \end{pmatrix}. \quad (3)$$

The model of (3) was validated experiments (see Fig. 6).

3) Low-Level Control Workflow and Hardware: To validate our proposed control method, we set up a pneumatic control board, as shown in Fig. 3(f). The pneumatic system of the control board consists of two pumps (KVP8S, Kamoer Inc.), two air tanks, and solenoid valves (OST Inc.) and an MCU of STM32F767 (ST Microelectronics Inc.) is used as the control unit of the system, and pressure sensors (SSCDANN060PAAA5, Honeywell Inc.) are used to provide pressure feedback. The board is set to receive a pressure command or valve action command, the control algorithm of pressure is shown in Fig. 3(g), which is also adopted in our previous work [20], [25], with a total system weight of 3.1 kg, including all necessary components, as shown in Fig. 3(f).

B. High-Level Control System of the Gripper

To validate the dexterity and passive-adaptability of our proposed gripper and showcase its benefit to ADL, we mounted two

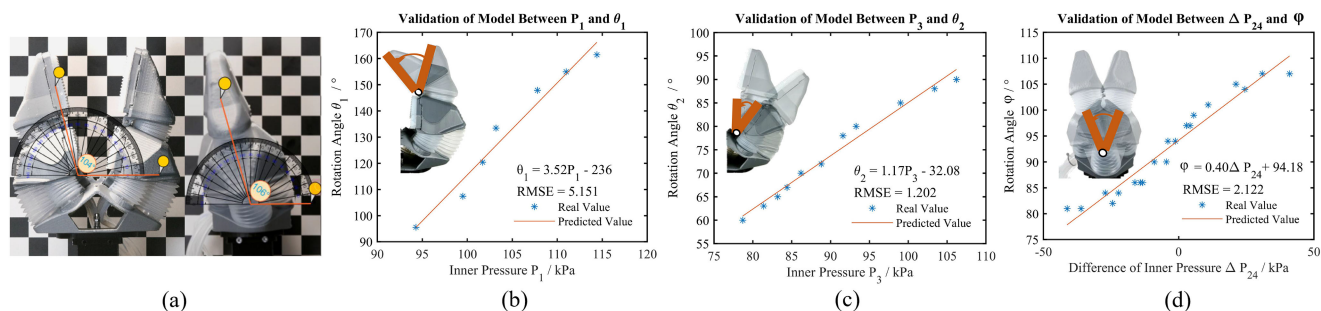


Fig. 6. Validation of each joint's linear characteristic between rotate angle and pressure. (a) Measurement method of rotation angle. (b) Tip joint in x - y plane. (c) Root joint in x - y plane. (d) Root joint in y - z plane.

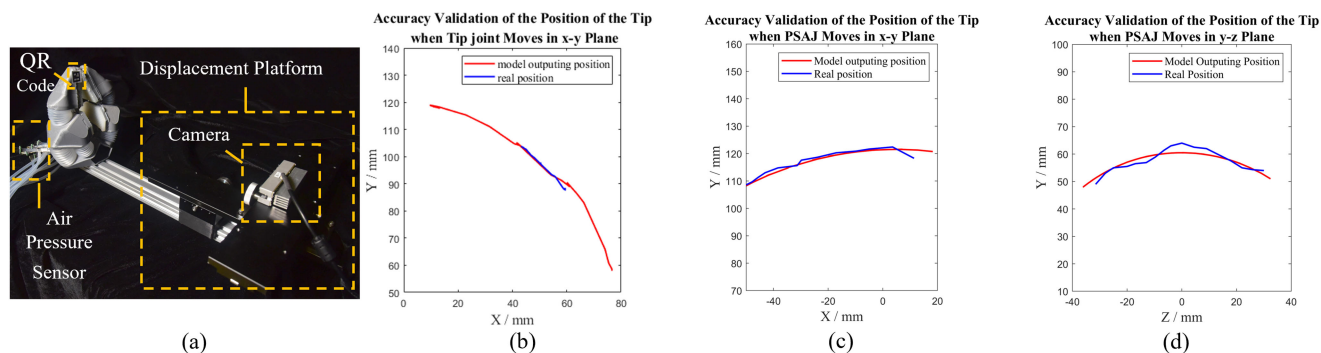


Fig. 7. Accuracy validation of each joint. (a) Experiment devices. A camera (Astra Mini Pro, ORBBEC Inc.) was employed to record the real position of the gripper tip and two high-precision optical displacement platforms (LWX60-L300, BEIAN Inc.) were used to provide x - y displacement of the camera. (b)–(d) Comparison of the real position recorded by the camera and the computing position put out from models in Fig. 6 of tip joint in the x - y plane, PSAJ in the x - y plane, and PSAJ in the y - z plane, respectively.

BHG-6 grippers on our proprietary high-level control system, including a dual-arm robot and RGB-D vision to provide perception for ADL tasking of soft, deformable and thin towel-like objects appressed on rigid surfaces, validating the compliance and passive adaptability of the gripper. A vision-based planning process was developed to integrate our proposed gripper into the high-level control workflow.

1) *Hardware Specification*: The hardware of the high-level control system is shown in Fig. 4(a). Grippers are installed as the end-effector of a dual-arm robot (KV220, Santifico) with 6 DOF for each arm. An RGB-D camera (Azure Kinect, Microsoft) was installed at the head of the dual-arm robot for object recognition and targeting.

2) *Simulation Model Setup of the Gripper*: To integrate the gripper into the unitive robot system Rviz and ROS [27] with the robot arm for visualization of controlling, we build the simulation model for the gripper in a hybrid structure. Different from soft grippers difficult to simulate with their soft-material body, hybrid grippers are easy to construct such a simulation model for their rigid-link structures can be modeled similarly to rigid-link grippers [28].

The model setup workflow of the gripper is shown in Fig. 4(b)–(d). The whole setup process can be separated into the modeling of rigid links and soft actuators, respectively. For rigid links, two fingers are modeled as two serial links connected to the same base link. For soft actuators, since their deformations could

be calculated analytically without requiring any simulation, we could simply use spheres to visualize their deformation at very low computational costs. During real-time gripper motion, the bottom sphere is fixed with the bottom link while the top sphere is fixed with the upper link, hence, the endpoint of the bellow can be determined. For the rest points, we use a linear model to approximately represent the point position. The distance of the sphere's center is determined by the deformed length of the soft actuator at each time instance for real-time rendering.

3) *Visual-Based Grasping Point Detection*: Acquisition of the grasping points is done through a five-step 2.5-D grasping point acquisition approach, and the edge detection of towel edge is determined using only one 2-D image at a time. The detailed process includes the following:

- 1) Collect the original image.
- 2) Extract the mask.
- 3) Segment region of interest (ROI).
- 4) Detect 2-D grasping points.
- 5) Calculate the actual grasping point position.

The vision-based grasping process is shown in Fig. 5. Due to the different colors of the object and background, the blue color of the towel is used as a feature to separate the ROI, and the mask range of the blue area is [100,100,50]-[130,255,255]. To obtain the minimum enclosing rectangle of ROI, the edge detection of ROI is carried out by the Canny operator [30]. The S2D grasping points are the center of the two sides of the towel.

TABLE II
COMPARISON OF THE PROPOSED GRIPPER AND SIMILAR WORKS

	BCL-4 [21]	BCL-6 [14]	iHY [29]	Three-finger compliant gripper [16]	Our proposed gripper
<i>Fingers</i>	2	3	3	3	2
<i>DOFs*</i>	4	6	9	6	6
<i>Self-weight</i>	0.2 kg	0.4 kg	1.5 kg	1.2 kg	0.39 kg (3.5 kg total)
<i>Grasping Force</i>	Joint: 50 N, Distal link: 12 N	40 N	220 N	42 N	Proximal link: 84.04 N, Distal Joint: 35.73 N, Distal link: 19.87 N,
<i>Maximum Grasping Force/Self-Weight</i>	25	10	14.67	3.5	21.55

*DOFs: The sum of DOF of all fingers.

After acquiring the grasping points, the coordinate is transformed from an image coordinate system to a world coordinate system for the following planning and grasping.

4) *Passive Adaptability to Grasp Against Rigid Surface*: Distinguish between a thin object made of soft materials, such as towel, and rigid surface, such as a table, utilizing vision is difficult due to the depth error (typically about 11 mm [31]) of vision system, which brings difficulties in grasping. Instead of using complex algorithms and expensive high-precision cameras to reduce error, grasping using lateral compliance of the gripper can greatly reduce the requirements for equipment and complex processes by setting the grasping point below the detected position for a distance covering detect error. According to this, we proposed a “poke and pinch” process to grasp the towel: Before grasping, the end-effector points are set to be above the detected grasping point, both actuators 2 and 4 were locked, with the gripper inclined to allow finger passively deform in a lateral direction at poking process.

As shown in Fig. 5(c), the gripper operates under Mode 2, opened prior to being pressed down against the rigid surface. The target of the gripper distal tip is set beneath the detected position for 20–30 mm, in order to ensure overpressing and deflect the gripper onto the surface. With lateral compliance, the PSAJ gripper could adapt passively, establishing contact with the towel while remaining open. Using Mode 2, the gripper closes the fingers to pinch the towel, then switches to Mode 3, to hold the grasping pressure while the gripper picks the towel up. The error tolerance under different approaching angles was analyzed experimentally in the next chapter.

IV. EXPERIMENTAL VALIDATION

A. Gripper Characteristic Validation

The comparison between the proposed BHG-6 gripper and other gripper designs in the literature is shown in Table II. From the comparison, the hybrid line of gripper designs had retained an excellent payload-weight ratio of around 20 times while obtaining additional dexterity with lateral compliance.

1) *Single Joint Characteristics*: The model between rotating angle and pressure was validated, as shown in Fig. 6(a). We placed the grippers before a calibration board and obtain the image of them, then corrected the distortion of the image. A visual protractor was used to measure the rotating angle of

joints, and then the relations between angles and joints proposed in (3) can be obtained and validated, which is used for the controlling of “FEAA mode.” Results have shown good linearity with curve fitting RMSE 5.151°, 1.202°, and 2.122°, respectively [see Fig. 6(b)–(d)].

2) *Gripper Accuracy Test*: We send different air pressure commands to each bellow and make the fingertips reach different positions. Use the camera to record the real position reached by the fingertip, and calculate the error with the position calculated from the model, as shown in Fig. 7(a). The comparisons of the real position and the modeled position are shown in Fig. 7(b)–(d). The positional error values of Fig. 7(b)–(d) are 1.57 mm, 1.82 mm, and 5.09 mm, respectively. We also estimated the tip accuracy using curve fitting RMSE of 3.39 mm (or 2%) in the main vertical plane, or 6.12 mm (or 3.7%) in the entire working space. Although the overall estimation accuracy does not compare directly against the 1% typically resulting from direct angular measurements, the 2–3% accuracy estimations from the proposed approach provided reasonable feedback information for object grasping, especially combining with the excellent passive compliance of soft actuators. The absolute error ranges of 3–6 mm are also well within the 10-mm vision accuracy level, as discussed in Section III-B.4, sufficient for this work.

3) *Gripper Payload Test*: The maximum load in different directions of the gripper was also validated, as shown in Fig. 8. The test apparatus includes a digital tension meter (ELK-500, ELECALL Inc., 500N max) capable of storing the peak tension. Connected to the tension meter is a small ball caught in the paws. At the same time, a rigid limit structure [see Fig. 8(b)] is installed on both sides of the gripper to restrict the lateral movement and to compare the advantages of adding lateral degrees of freedom.

The load plots in Fig. 8(e) show the gripper was able to carry load 21.5 times its self-weight; in contrast, the load capacity was reduced to less than 50 N when the lateral DOF was deleted, 53.5 N lower than the former situation. This was largely due to the lateral compliance enabled by the PSAJ joint, allowing the gripper to deflect toward the force loading direction, significantly improving the grasping envelop. As grasping is most secure with the PIP and MCP joints both wrapping around the ball, enhancing friction on the silicone rubber soft contact layer against external pulling forces, this passive adaptation resulted in substantially higher pull-out forces, of 87.3% over the case when lateral compliance was restricted by the limiter.

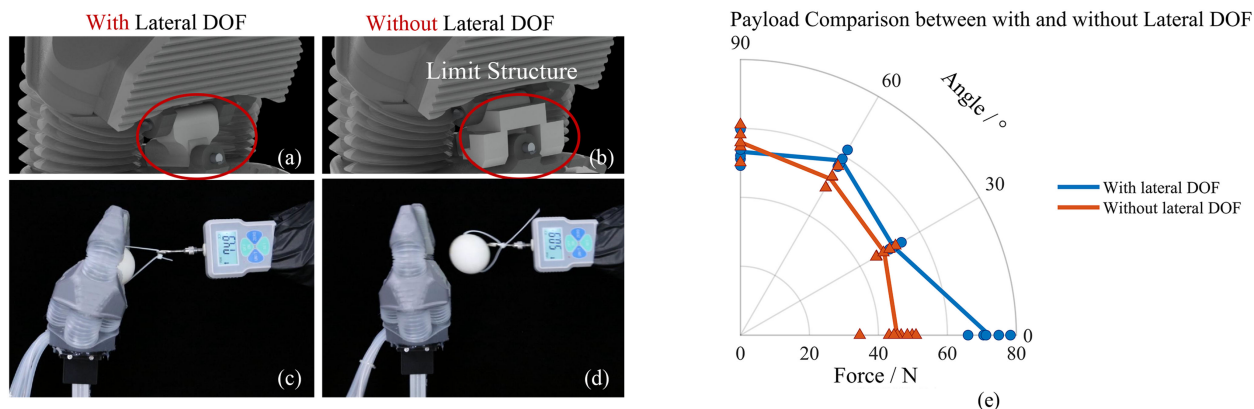


Fig. 8. Lateral payload test experiments. (a) and (b) Comparison of structures that limit the lateral DOF and not. (a) It uses the universal pin hinge to provide 2 DOFs. (b) It uses limit structure to remove lateral DOF. (c) Payload-test experiments with lateral DOF. (d) Payload-test experiments without lateral DOF. (e) Experiment result of payload with and without lateral DOF.

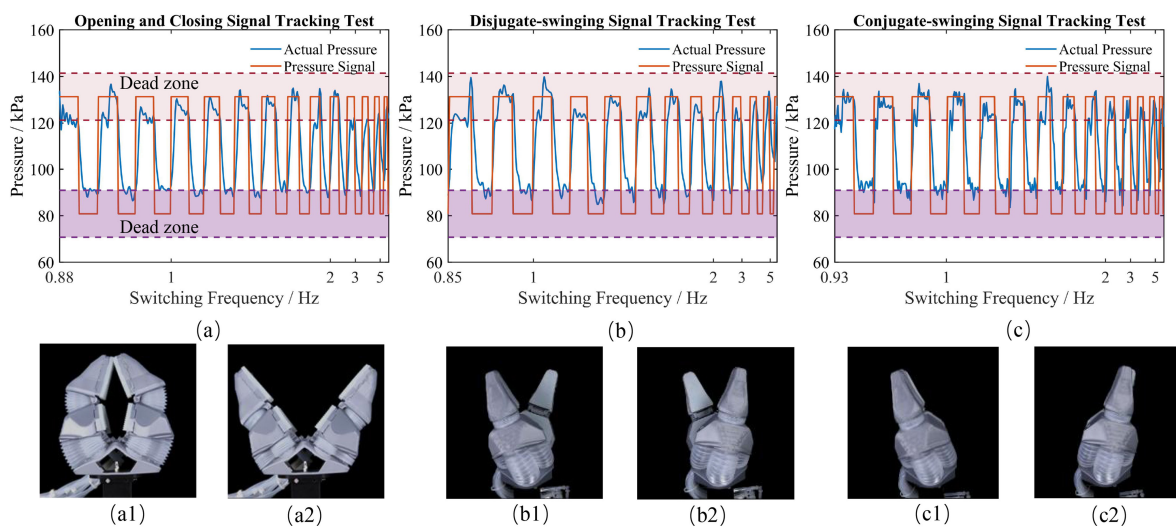


Fig. 9. Tracking performance test. (a) Tracking performance when gripper is opening and closing in continuous circulation. (b) Tracking performance when gripper circulates in the same direction simultaneously. (c) Tracking performance when gripper continuously rotates in opposite directions.

4) *Tracking Performance*: Three different commands were used in driving the actuators to assess the tracking performance of the control system.

Group1: the left-side gripper and right-side gripper are simultaneously opening and closing.

Group2: the left-side gripper and right-side gripper are simultaneously swinging in the same direction.

Group3: the left-side gripper and right-side gripper are simultaneously swinging in different directions.

The target pressure control frequency was increased gradually to test the control bandwidth. The interval of each group starts at 1.3 s, reduces to 0.08 s each time after a wave, and end while the interval is smaller than 0.2 s.

As can be seen from Fig. 9, with an increasing reference pressure frequency, the pressure could reach the reference at least once during the cycle for frequencies up to 5 Hz, apparently higher than present soft-bodied grippers [32], [33].

B. Gripper Performance Validation

1) *In-Hand Manipulation*: Experiments were carried out to test the gripper's grasping adaptability, as shown in Fig. 10. We prepared three grabbing items with different shapes. For smaller-sized wires, the gripper uses fingertips to grab; for medium-sized glue bottle, the gripper uses the middle of the finger to grab; for a larger sized beverage bottle, the gripper uses the finger base to grab it [see Fig. 10(a)–(c)]. In Fig. 10(d) and (e), the gripper rotates a 10-cm ball around the orthogonal vertical and lateral axis. In Fig. 10(f), the gripper wiggles a pen with its lateral DOFs.

2) *Water-Pouring Using Only In-Hand DOFs*: As an integrated demonstration, the gripper was used to pour a cup of water while the robotic manipulator was fixed without moving. The pouring was entirely carried out by the gripper inclining the cup downward using its lateral DOF in the BSAJ joints [see Fig. 11(a)].

3) *Grasping Water Cup Utilizing Model*: An experiment is carried out to validate our model in practical application. As

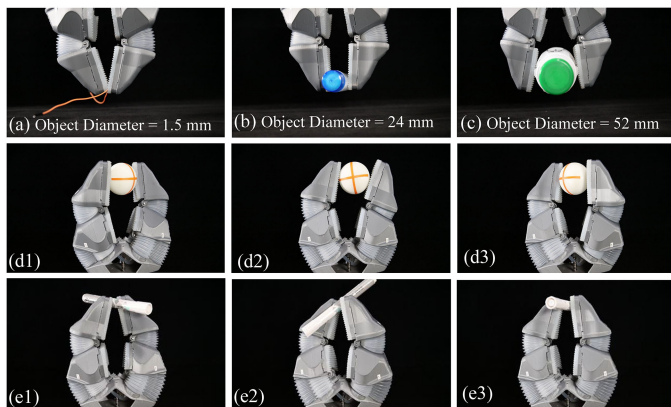
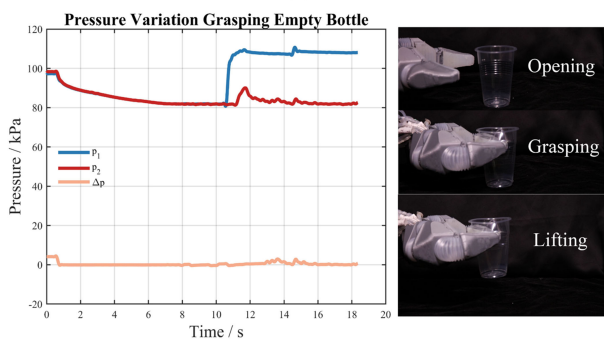


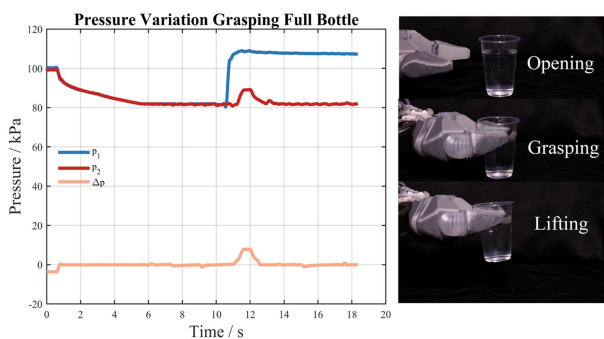
Fig. 10. In-hand manipulation experiments. (a) Grasping a wire. (b) Grasping a glue bottle. (c) Grasping a beverage bottle. (d) In-hand rotation of rolling a ball. (e) In-hand translation of rolling a ball. (f) In-hand rotation of rolling a pen.



(a)



(b)



(c)

Fig. 11. (a) Pouring water procedure. It is important to note that there is no wrist movement in this figure. (b) Grasping empty bottle. (c) Grasping bottle full of water.

shown in Fig. 11(b) and (c), we grasp two types of water cups, one filled with water and one empty, using the same pressure value. The pressure value is calculated according to the diameter of the water cup. The diameter of the cup is 27 mm. The grasp point is set to be the middle of the cup. Hence, the x coordinate of the grasping point is -9.6 mm. Then, we can calculate the correspondent angle of each joint θ_1 , θ_2 , and φ to be 145, 62, and 0, respectively. According to the model, the pressure will be 108.28, 80, and 0 kPa, respectively. Although the position control may not be accurate, the results show that it can stably grasp the soft water cup, both the empty one and the full one.

C. Dual-Gripper Object Handling

1) *Towel Folding Performance*: Fig. 11 shows the proposed grasping pipeline applied to picking up a towel using dual BHG-6 grippers. Once a towel is grasped and lifted with the robotic arms [see Fig. 12(a)], the folding process starts. The whole procedure is performed by two grippers until the left gripper moves away with holding the whole towel [see Fig. 12(d)]. To showcase the capability of the added lateral compliance, the entire handing-over procedure of the towel was performed purely via in-hand manipulation of the grippers, without moving the arms. The full procedure is included in the supplemented video.

2) *Lateral Compliance*: To further demonstrate the benefit of adding lateral compliance to dual-gripper object handling, a manipulation setup was created with the grippers holding onto a rigid rod with a force/torque sensor mounted in the middle to measure the manipulation forces. As shown in Fig. 13, the object is composed of two aluminum rods, and a 6-DOF force sensor (ATI Nano17, ATI Inc.) mounted in between.

The experiments were divided into four different modes, as shown in Fig. 13(b)–(e): lateral compliance enabled on both ends; lateral compliance enabled only on the pulling end; lateral compliance enabled only on the recipient end; no lateral compliance on either end. The results are shown in Fig. 13(a). For the group without lateral freedom, the stress of this group is the largest and the rising slope is the largest. For the mode with single lateral freedom, the stress is only that there is no lateral freedom. For the group with 2 DOF, the stress is only 47.2% of the one-sided degrees of freedom and 10.6% of the group without lateral degrees of freedom. Enable lateral compliance, therefore, could effectively and substantially reduce closed-loop stress and enable the proposed PSAJ gripper to handle rigid objects bimanually without risking any damage or instability. But due to slight misalignments between the two grasping positions between each trial, the pulling directions may be slightly misaligned, causing discrepancies in the slopes of Fig. 13(c) and (d).

3) *Lateral Compliance for Object Picking From Rigid Surfaces*: Finally, the capability of the proposed PSAJ gripper in picking up flat soft objects against rigid surfaces was assessed. The experiment was divided into five conditions, where the gripper approached the rigid surface from different angles (015° , 30° , 45° , and 60° , respectively). In each condition, the arm was descended vertically until the gripper is deformed to a maximum allowable position against the rigid surface below.

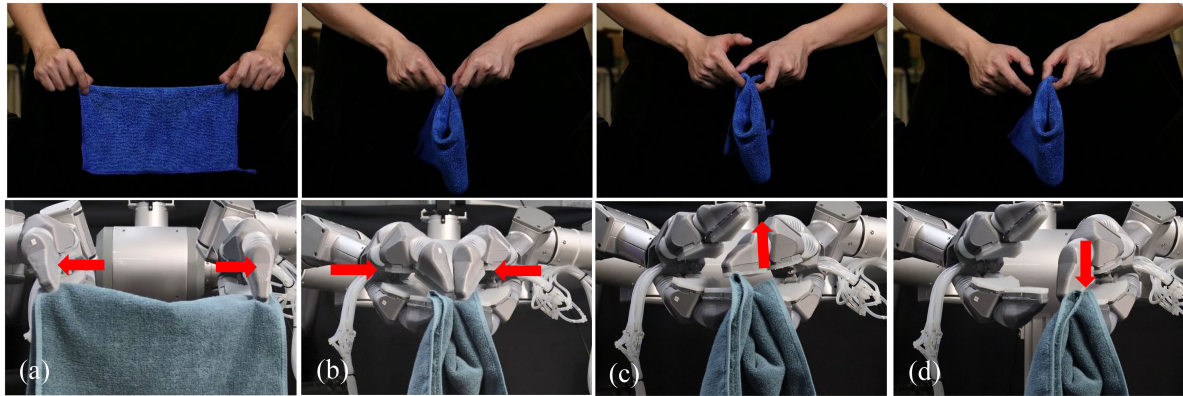


Fig. 12. Complete pipeline of folding a towel. (a) Towel was successfully picked up by grippers. (b) Fold the towel with two grippers. (c) Loose the towel from the upper left gripper. (d) Grab the towel with the right gripper and move away.

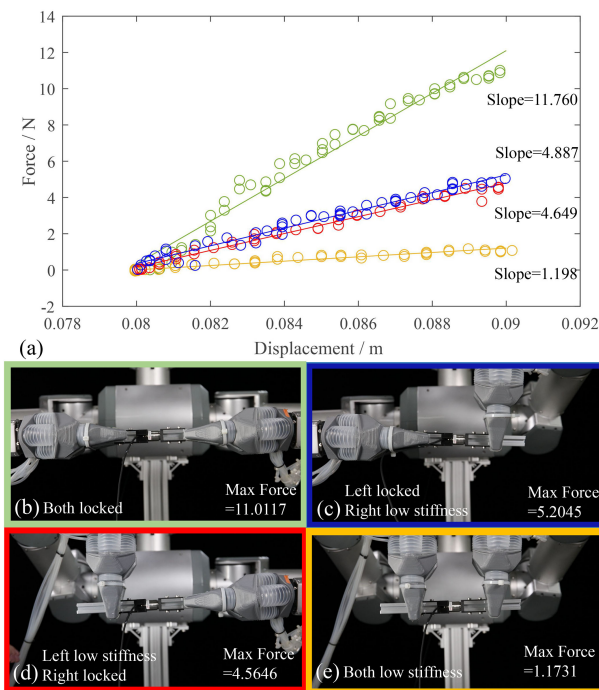


Fig. 13. Lateral compliance experiments. (a) Relationship between pulling force and pulling displacement of each experiment. (b)–(e) Pulling aluminum alloy rod with two arms.

As shown in Fig. 13, the gripper reached down and grabbed the towel at different approaching angles, the maximum tolerated error was recorded, where the gripper could still pick up the towel successfully. It could be observed from the results that the fault tolerance is greatest when the gripper is at 45°, and decreases when the angle both increases and decreases, mostly due to the mechanistic constraint of the rigid links, where the soft actuator's compliance will be hindered and even eliminated when being fully compressed between two mounting rigid parts. At the same time, the results in Fig. 14 highlighted the excellent passive adaptability of the PSAJ gripper against environmental interaction uncertainties, enabling the gripper to effectively pick up a very thin and soft object (a towel, in this case, under

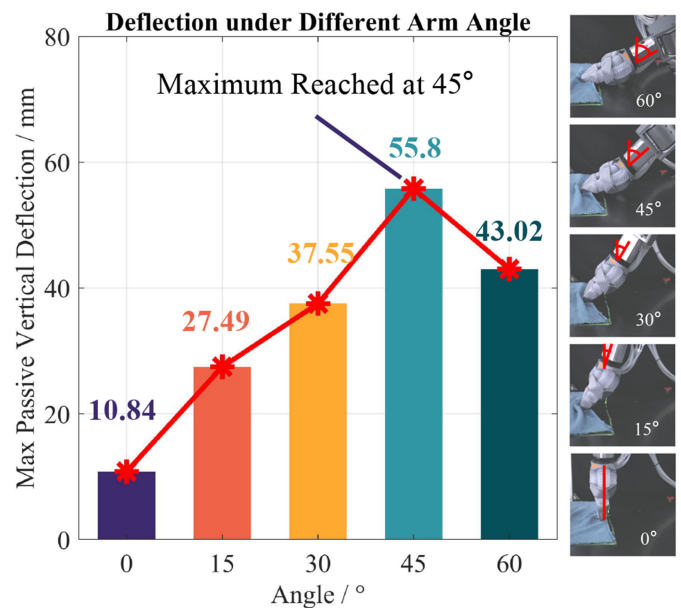


Fig. 14. Lateral compliance experiments. The gripper grasps the towel at 0°, 15°, 30°, 45°, 60°, and 90° inclines, respectively.

inaccurate position detection due to camera error), from a rigid desk.

V. CONCLUSION

In this article, a two-finger hybrid gripper design was proposed with 6 DOFs, based on a synergistic PSAJ hybrid joint design, actuated by 8 independent pneumatic soft muscles augmented into rigid constraining structures. The gripper had both flexion/extension and abduction/adduction enabled on the proximal joint, and flexion/extension on the distal joint. It was shown that adding the MCP complexity with a synergistic muscle configuration was effective in enabling a range of novel manipulation and compliant features in the hybrid gripper, as well as new control modes. A prototype gripper was fabricated and tested on our proprietary dual-arm robot platform with vision-guided grasping. With very lightweight pneumatic bellows soft

actuators, the gripper could grasp objects over 20 times its own weight (or 2.4 times with the entire pneumatic control system included) with lateral compliance.

Kinematic modeling was performed to describe the motion of the gripper. A multimode method is proposed to enable the gripper to have the ability to grasp and operate a wide range of objects and complete dexterous tasks. The load test showed the lateral DOF provides 59.1 N more than without lateral DOF. For dual-arm manipulation capability, the grippers are proved for complex tasks, such as folding towels, and the lateral stiffness can also reduce the stress by over 70%. Utilizing the gripper's lateral compliance, a list of interactive features was demonstrated, from reducing closed-loop stress, to adapting to a vertical error during thin object picking against rigid surfaces. The PSAJ gripper, completed with modeling and the overall dual-arm system demonstration, offers a high-performance alternative to a compliant gripper design.

Future works will focus on mechanical design refinements, including different dimensions and materials; higher level control iterations; higher accuracy grasping as well as adding sensors, such as angle encoder, to improve grasping accuracy and sensing modalities to improve interactive intelligence. This work paves the way to soft-rigid hybrid grippers with a strategically balanced blend of simplicity, adaptability, and dexterity.

ACKNOWLEDGMENT

The authors would like to thank Mr. K. Zou for setting up the hardware of the control device, Ms. Y. Ding for video editing, and Ms. Y. Cheng for casting the silicone layer of the gripper.

REFERENCES

- [1] J. Shintake, V. Cacucciolo, D. Floreano, and H. Shea, "Soft robotic grippers," *Adv. Mater.*, vol. 30, no. 29, Jul. 2018, Art. no. 1707035.
- [2] K. Yamazaki et al., "Home-assistant robot for an aging society," *Proc. IEEE*, vol. 100, no. 8, pp. 2429–2441, Aug. 2012.
- [3] I. M. Bullock, R. R. Ma, and A. M. Dollar, "A hand-centric classification of human and robot dexterous manipulation," *IEEE Trans. Haptics*, vol. 6, no. 2, pp. 129–144, Apr.–Jun. 2013.
- [4] A. Billard and D. Kragic, "Trends and challenges in robot manipulation," *Science*, vol. 364, Jun. 2019, Art. no. eaat8414.
- [5] M. T. Mason, "Toward robotic manipulation," *Annu. Rev. Control, Robot., Auton. Syst.*, vol. 1, pp. 1–28, 2018.
- [6] S. Qiao et al., "Configuration design of an under-actuated robotic hand based on maximum grasping space," *Chin. J. Mech. Eng.*, vol. 31, no. 35, 2018, Art. no. 35.
- [7] C. Liu et al., "Design of a self-adaptive gripper with rigid fingers for industrial internet," *Robot. Comput.-Integr. Manuf.*, vol. 65, 2020, Art. no. 101976.
- [8] Z. Zhang, T. Han, J. Pan, and Z. Wang, "Design of anthropomorphic fingers with biomimetic actuation mechanism," *IEEE Robot. Automat. Lett.*, vol. 4, no. 4, pp. 3465–3472, Oct. 2019.
- [9] Shadow Robot Company, "Shadow dexterous hand technical specification," Jun. 2012. [Online]. Available: http://mindtrans.narod.ru/pdfs/shadow_dextrous_hand_technical_specification_C6M_20120627.pdf
- [10] A. M. Dollar and R. D. Howe, "The highly adaptive SDM hand: Design and performance evaluation," *Int. J. Robot. Res.*, vol. 29, no. 5, pp. 585–597, 2010.
- [11] T. Chen, L. Wang, M. Haas-Heger, and M. Ciocarlie, "Underactuation design for tendon-driven hands via optimization of mechanically realizable manifolds in posture and torque spaces," *IEEE Trans. Robot.*, vol. 36, no. 3, pp. 708–723, Jun. 2020.
- [12] F. Ilievski et al., "Soft robotics for chemists," *Angewandte Chemie*, vol. 50, no. 8, pp. 1890–1895, 2011.
- [13] E. Brown et al., "Universal robotic gripper based on the jamming of granular material," *Proc. Nat. Acad. Sci. USA*, vol. 107, pp. 18809–18814, 2010.
- [14] J. Zhou, S. Chen, and Z. Wang, "A soft-robotic gripper with enhanced object adaptation and grasping reliability," *IEEE Robot. Automat. Lett.*, vol. 2, no. 4, pp. 2287–2293, Oct. 2017.
- [15] J. Yi, X. Chen, C. Song, and Z. Wang, "Fiber-reinforced origamic robotic actuator," *Soft Robot.*, vol. 5, pp. 81–92, 2018.
- [16] C. H. Liu, F. M. Chung, Y. Chen, C. H. Chiu, and T. L. Chen, "Optimal design of a motor-driven three-finger soft robotic gripper," *IEEE/ASME Trans. Mechatronics*, vol. 25, no. 4, pp. 1830–1840, Aug. 2020.
- [17] Z. Xie, F. Yuan, Z. Liu, Z. Sun, E. M. Knubben, and L. Wen, "A proprioceptive soft tentacle gripper based on crosswise stretchable sensors," *IEEE/ASME Trans. Mechatronics*, vol. 25, no. 4, pp. 1841–1850, Aug. 2020.
- [18] S. Liu, F. Wang, Z. Liu, W. Zhang, Y. Tian, and D. Zhang, "A two-finger soft-robotic gripper with enveloping and pinching grasping modes," *IEEE/ASME Trans. Mechatronics*, vol. 26, no. 1, pp. 146–155, Feb. 2021.
- [19] Y. Li, Y. Chen, Y. Yang, and Y. Li, "Soft robotic grippers based on particle transmission," *IEEE/ASME Trans. Mechatronics*, vol. 24, no. 3, pp. 969–978, Jun. 2019.
- [20] S. Liu et al., "Otariidae-inspired soft-robotic supernumerary flippers by fabric kirigami and origami," *IEEE/ASME Trans. Mechatronics*, vol. 26, no. 5, pp. 2747–2757, Oct. 2021.
- [21] J. Zhou, X. Chen, J. Li, Y. Tian, and Z. Wang, "A soft robotic approach to robust and dexterous grasping," in *Proc. IEEE Int. Conf. Soft Robot.*, 2018, pp. 412–417.
- [22] D. Drotman, M. Ishida, S. Jadhav, and M. T. Tolley, "Application-driven design of soft, 3-D printed, pneumatic actuators with bellows," *IEEE/ASME Trans. Mechatronics*, vol. 24, no. 1, pp. 78–87, Feb. 2019.
- [23] J. Zhou, Y. Chen, X. Chen, Z. Wang, Y. Li, and Y. Liu, "A proprioceptive bellows (PB) actuator with position feedback and force estimation," *IEEE Robot. Automat. Lett.*, vol. 5, no. 2, pp. 1867–1874, Apr. 2020.
- [24] J. Yi, X. Chen, C. Song, J. Zhou, Y. Liu, and Z. Wang, "Customizable three-dimensional-printed origami soft robotic joint with effective behavior shaping for safe interactions," *IEEE Trans. Robot.*, vol. 35, no. 1, pp. 114–123, Feb. 2019.
- [25] Y. Su et al., "A high-payload proprioceptive hybrid robotic gripper with soft origamic actuators," *IEEE Robot. Automat. Lett.*, vol. 5, no. 2, pp. 3003–3010, Apr. 2020.
- [26] L. Wang and Z. Wang, "Mechanoreception for soft robots via intuitive body cues," *Soft Robot.*, vol. 7, pp. 198–217, Apr. 2020.
- [27] M. Quigley, "ROS: An open-source robot operating system," in *Proc. Int. Conf. Robot. Automat. Workshop Open Source Softw.*, vol. 3, no. 3.2, 2009.
- [28] J. Chen, H. Deng, W. Chai, J. Xiong, and Z. Xia, "Manipulation task simulation of a soft pneumatic gripper using ROS and Gazebo," in *Proc. IEEE Int. Conf. Real-Time Comput. Robot.*, 2018, pp. 378–383.
- [29] L. Odhner et al., "A compliant, underactuated hand for robust manipulation," *Int. J. Robot. Res.*, vol. 33, no. 5, pp. 736–752, 2014.
- [30] J. Canny, "A computational approach to edge detection," *IEEE Trans. Pattern Anal. Mach. Intell.*, vol. PAMI-8, no. 6, pp. 679–698, Nov. 1986.
- [31] Microsoft, "Azure Kinect DK hardware specifications," Mar. 2021. [Online]. Available: <https://docs.microsoft.com/en-us/azure/Kinect-dk/hardware-specification>
- [32] M. A. Robertson and J. Paik, "Low-inertia vacuum-powered soft pneumatic actuator coil characterization and design methodology," in *Proc. IEEE Int. Conf. Soft Robot.*, 2018, pp. 431–436.
- [33] C. Tawk, A. Gillett, M. in het Panhuis, G. M. Spinks, and G. Alici, "A 3D-printed omni-purpose soft gripper," *IEEE Trans. Robot.*, vol. 35, no. 5, pp. 1268–1275, Oct. 2019.



arm manipulator.

Wenpei Zhu received the B.S. degree in mechanical engineering from the Hefei University of Science and Technology, Hefei, China, in 2018. He is currently working toward the master's degree majoring in electronic science and engineering with the Department of Mechanical and Energy Engineering, Southern University of Science and Technology, Shenzhen, China.

He is currently with the BioRobotics and Control Laboratory. His research interests include control and modeling of soft robotics and dual-



Chenghua Lu received the B.S. degree in mechanical engineering from Northeastern University, Shenyang, China, in 2017, and the M.S. degree in mechanical manufacturing and automation from the University of Chinese Academy of Sciences, Beijing, China, in 2021.

She is currently a Research Assistant with the BioRobotics and Control Laboratory, Southern University of Science and Technology, Shenzhen, China. Her research interests include soft hand design, control algorithm optimization, and cooperative robot control.



Qule Zheng received the B.S. degree in electronic and information engineering from Northwest A&F University, Xianyang, China, in 2017, and the M.S. degree in aerospace engineering from Xidian University, Xi'an, China, in 2020. She is currently working toward the Ph.D. degree majoring in mechanics with the Department of Mechanical and Electrical Engineering, Harbin Institute of Technology, Shenzhen, China.

She is currently with the BioRobotics and Control Laboratory. Her research interests include digital image processing and computer vision.



Zhonggui Fang received the B.S. degree in mechanical design manufacturing and automation from the Guangdong University of Technology, Guangzhou, China, in 2019. He is currently working toward the M.S. degree majoring in mechanics with the Department of Mechanical Engineering and Energy Engineering, Southern University of Science and Technology, Shenzhen, China.

His research interests include soft robotics for medical application and wearable robots.



Haichuan Che is currently working toward the B.S. degree majoring in mechanical engineering with the Department of Mechanical and Engineering, Southern University of Science and Technology, Shenzhen, China.

He is currently with the BioRobotics and Control Laboratory. His research interests include soft robotics and robot arm manipulation.



Kailuan Tang received the B.S. degree in communication engineering from the Southern University of Science and Technology, Shenzhen, China, in 2017. He is currently working toward the Ph.D. degree majoring in mechanics with the Department of Mechanical and Electrical Engineering, Harbin Institute of Technology, Shenzhen, China.

He is currently with the BioRobotics and Control Laboratory. His research interests include underwater robots, biomimetic control, and soft

robots.



Mingchao Zhu received the B.S. degree in automation and the Ph.D. degree in control theory and control engineering from Jilin University, Changchun, China, in 2003 and 2009, respectively.

He is currently a Researcher with the Changchun Institute of Optics, Fine Mechanics and Physics, Chinese Academy of Sciences, Changchun, China. He is also a Master Supervisor with the University of Chinese Academy of Sciences, Beijing, China. His research interests

include kinematics, dynamics, and robot control.



Sicong Liu received the B.S. (Hons.) degree in mechanical design manufacturing and automation and the M.S. degree in mechanical design and theory from the Harbin Institute of Technology, Harbin, China, in 2009 and 2011, respectively, and the Ph.D. degree in robotics and engineering mechanics from Nanyang Technological University, Singapore, in 2015.

In 2016, he was a Postdoctoral Research Fellow with Nanyang Technological University. He was a Mechanical Engineer with DJI in 2017.

Then, he was a Senior Mechanical Engineer with UBTECH in 2019. He is currently a Research Assistant Professor with the Department of Mechanical and Energy Engineering and the Institute of Robotics, Southern University of Science and Technology, Shenzhen, China. His research interests include deployable structures inspired by origami and soft robotics.



Zheng Wang (Senior Member, IEEE) received the B.Sc. (Hons.) degree in automatic control from Tsinghua University, Beijing, China, in 2004, the M.Sc. (Hons.) degree in control systems from Imperial College London, London, U.K., in 2005, and the Ph.D. (Hons.) degree in electrical engineering from the Technische Universität München, Munich, Germany, in 2010.

He was a Postdoctoral Research Fellow with Nanyang Technological University, Singapore, from 2010 to 2013, and a Postdoctoral Fellow

with the School of Engineering and Applied Sciences and the Wyss Institute of Bioinspired Engineering, Harvard University, in 2013 and 2014, respectively. Since July 2014, he has been an Assistant Professor with the Department of Mechanical Engineering, The University of Hong Kong, Hong Kong. He has been a Professor in robotics with the Department of Mechanical and Energy Engineering, Southern University of Science and Technology, Shenzhen, China, since February 2019. His research interests include haptics human–robot interaction, endoscopic surgical robot, underwater robots, and soft robotics.